HHS Public Access

Author manuscript

J Magn Reson Imaging. Author manuscript; available in PMC 2021 October 08.

Published in final edited form as:

J Magn Reson Imaging. 2019 November ; 50(5): 1468–1477. doi:10.1002/jmri.26732.

Characterization of Sub-1 cm Breast Lesions Using Radiomics Analysis

Peter Gibbs, PhD[*], **Natsuko Onishi, MD, PhD**, **Meredith Sadinski, PhD**, **Katherine M. Gallagher, MD**, **Mary Hughes, MD**, **Danny F. Martinez, MS**, **Elizabeth A. Morris, MD**, **Elizabeth J. Sutton, MD**

Breast Imaging Service, Department of Radiology, Memorial Sloan Kettering Cancer Center, New York, New York, USA

Abstract

Background: Small breast lesions are difficult to visually categorize due to the inherent lack of morphological and kinetic detail.

Purpose: To assess the efficacy of radiomics analysis in discriminating small benign and malignant lesions utilizing model free parameter maps.

Study Type: Retrospective, single center.

Population: In all, 149 patients, with a total of 165 lesions scored as BI-RADS 4 or 5 on MRI, with an enhancing volume of <0.52 cm^3.

Field Strength/Sequence: Higher spatial resolution T_1-weighted dynamic contrast-enhanced imaging with a temporal resolution of ~90 seconds performed at 3.0T.

Assessment: Parameter maps reflecting initial enhancement, overall enhancement, area under the enhancement curve, and washout were generated. Heterogeneity measures based on first-order statistics, gray level co-occurrence matrices, run length matrices, size zone matrices, and neighborhood gray tone difference matrices were calculated. Data were split into a training dataset (~75% of cases) and a test dataset (~25% of cases).

Statistical Tests: Comparison of medians was assessed using the nonparametric Mann–Whitney *U*-test. The Spearman rank correlation coefficient was utilized to determine significant correlations between individual features. Finally, a support vector machine was employed to build multiparametric predictive models.

Results: Univariate analysis revealed significant differences between benign and malignant lesions for 58/133 calculated features ($P < 0.05$). Support vector machine analysis resulted in areas under the curve (AUCs) ranging from 0.75–0.81. High negative (>89%) and positive predictive values (>83%) were found for all models.

Data Conclusion: Radiomics analysis of small contrast-enhancing breast lesions is of value. Texture features calculated from later timepoints on the enhancement curve appear to offer limited

[*]Address reprint requests to: P.G., Breast Imaging Service, Department of Radiology, Memorial Sloan Kettering Cancer Center, 300 East 66th St., New York, NY, 10065. gibbsp@mskcc.org.

additional value when compared with features determined from initial enhancement for this patient cohort.

Level of Evidence: 4

Technical Efficacy: Stage 2

Since at least the 1960s the association between the size of a primary breast tumor and the prevalence of metastases has been well established,[1–3] clearly indicating the need to detect and characterize small breast lesions accurately. A very recent study[4] found in a cohort of 819,467 women that a nonlinear relationship exists between increasing tumor size and node-positive prevalence as well as the 15-year rate of breast cancer-specific mortality. However, the detection of early breast cancer remains a major challenge, since small cancers are generally less conspicuous on mammography.

Dynamic contrast-enhanced magnetic resonance imaging (DCE- MRI) has very high sensitivity (>90%) and reasonable specificity (>70%) in the characterization of general breast lesions.[5,6] It has poorer specificity in smaller lesions due to the reduced ability to visually distinguish morphological and kinetic features associated with malignancy, including the presence of an irregular lesion border and heterogeneous internal enhancement. Schlossbauer et al[7] summarized MRI dynamic and morphologic criteria in a diagnostic score and they concluded that score differences between benign and malignant lesions were reduced in lesions smaller than 1 cm in size. Other work indicates that cancers less than 1 cm become more obviously malignant as they enlarged, and that cancers less than 5 mm had benign characteristics.[8] As MRI screening is becoming more widespread for selected high-risk populations, it has been noted in this population that the majority of invasive carcinomas detected via this route are smaller than 1 cm in size.[9] Lesions regarded as suspicious (categorized as Breast Imaging-Reporting and Data System [BI-RADS] 4 or 5) are usually recommended for biopsy,[10] and since a higher percentage of smaller lesions are known to be benign,[11] this can potentially lead to a large number of negative biopsies, and thus a low positive predictive value.

Texture analysis, which involves quantitative assessment of the pixel intensity arrangement within specific regions of interest, has previously been employed in general breast MRI. Early work utilized parameters calculated from gray level co-occurrence matrices to discriminate between benign and malignant lesions.[12] Subsequent studies have incorporated more complex measures of image texture to both aid diagnosis[13] and to explore the efficacy of texture analysis in prognosis.[14–16]

The pool of literature that specifically focuses on the characterization of small breast lesions utilizing MRI remains limited. Early work assessed morphologic and kinetic characteristics in a cohort of 43 patients with sub-1 cm lesions.[17] The incorporation of either heuristic parameters, derived from enhancement within the first minute of contrast injection, or kinetic parameters calculated using a two-compartment pharmacokinetic model revealed a high diagnostic accuracy (area under the curve, AUC = 0.92). However, validation of this model in a second independent cohort was not performed. A further study investigated the classification performance of a model using texture features, whereby the features

were extracted from five postcontrast phases and then combined to form feature vectors, in 60 lesions with a mean lesion diameter of 1.1 cm.[18] The highest AUC value was achieved when incorporating texture features responsible for capturing various aspects of lesion heterogeneity (AUC = 0.82). Nagarajan et al[19] also explored the use of topological features determined from Minkowski functionals in small breast lesions and determined that perimeter assessment is of value. Recent work investigated the efficacy of more rapid sampling during the early portion of the contrast enhancement curve for the diagnosis of sub-1 cm diameter breast lesions.[20] The logistic regression model developed incorporated patient age, maximum slope, and bolus arrival time, achieving an AUC of 0,85.

Our study was undertaken to examine the utility of radiomic features extracted from model free parameter maps, based on high-resolution postcontrast scans, in the differentiation of benign and malignant lesions smaller than 0.52 cm^3 in volume (equivalent to a sphere of 1 cm diameter) on presentation at MRI.

Materials and Methods

This retrospective Health Insurance Portability and Accountability Act (HIPAA)-compliant study received Institutional Review Board approval and the need for informed consent was waived. A retrospective review of patients imaged between February 2017 and January 2018 was performed to identify eligible cases. Inclusion criteria were lesions scored as BI-RADS 4 or 5 on MRI, and an enhancing volume of <0.52 cm^3. Exclusion criteria included postchemotherapy treatment response assessment examinations and cases with no pathological diagnosis. In all, 149 patients, with a total of 165 lesions, fulfilled the inclusion criteria. The median age was 48 years (range 19–79 years). There were 130 benign lesions (with 16 categorized as high-risk benign lesions) and 35 malignant lesions. Further lesion characteristics are provided in Table 1. The data were split into a training dataset of 124 lesions (98 benign and 26 malignant lesions) and a test dataset of 41 lesions (32 benign and 9 malignant).

All MRIs were performed using a 3.0T scanner (GE Discovery 750, GE, Milwaukee, WI) with a dedicated 8- or 16-channel breast coil. A high spatial resolution T_1-weighted scan was acquired precontrast injection. As part of a separate study investigating the utility of a high temporal resolution view-sharing method in the diagnosis of breast lesions, a differential subsampling with Cartesian ordering (DISCO) technique was employed for the first 60 seconds following contrast injection (0.1 mmol gadobutrol/kg body weight). Subsequently, conventional steady-state DCE high spatial resolution (1.1 mm isotropic) images were acquired with a temporal resolution of ~90 seconds for three phases (Table 2). Example higher-resolution images utilized in feature calculation are illustrated in Fig. 1.

After data acquisition, DCE images were visually assessed by a radiologist (N.O.) to exclude cases with evidence of significant motion between phases. Lesions were identified by a radiologist with 7 years' experience of breast MR, and subsequently manually segmented by a researcher with over 20 years' experience in breast MRI on the first higher-resolution postcontrast images. Segmentation was performed across all lesion containing slices and the volume of interest subsequently transferred to the pre- and remaining postcontrast phases.

Parameter maps quantifying the initial enhancement, overall enhancement, washout, and area under the enhancement curve were calculated pixel-by-pixel as follows:

$$Initial\ Enhancement = 100 \times \frac{S_1 - S_0}{S_0}$$

$$Overall\ Enhancement = 100 \times \frac{S_3 - S_0}{S_0}$$

$$Washout = 100 \times \frac{S_3 - S_1}{S_1}$$

$$AUC = \int_{i=1}^{3} \frac{S_i - S_0}{S_0}$$

where S_i represents the signal in the ith postcontrast phase, and S_0 represents the signal in the precontrast phase.

Region of interest (ROI) data were reduced to 16 gray levels on a per-lesion basis. This ensured reasonable counting statistics for subsequent texture feature calculations. Features based on first-order statistics (variance, skewness, kurtosis, energy, entropy) were initially determined. Two-dimensional gray level co-occurrence matrices (GLCMs) were calculated for a separation of 1 pixel, utilizing four different directions (0°, 45°, 90°, 135°). Fourteen texture features as detailed by Haralick et al[21] were calculated, alongside cluster shade and cluster prominence as proposed by Conners et al,[22] and subsequently averaged across the four directions since there is no expectation of preferred directionality in the texture features. Eleven texture features based on run length matrices[23] were calculated for the four different directions and similarly averaged. Run length matrices give the size of homogeneous runs for each gray level and the calculated parameters reveal the importance of short runs, long runs, low gray values, and high gray values in various combinations. Eleven features based on size zone matrices[24] were also calculated. Finally, neighborhood gray tone difference matrices[25] were determined and from these the features coarseness, contrast, busyness, complexity, and texture strength calculated. Thus, texture analysis resulted in 48 features for each of the four distinct heuristic parameter maps.

Statistical Analysis

The data were split into a training dataset (~75% of cases) and a test dataset (~25% of cases). All model development was performed on the training dataset and the test dataset was only utilized for final model assessment. Univariate analysis was initially employed to explore significant differences between benign and malignant lesions. Due to the relatively low number of malignant lesions the nonparametric Mann–Whitney U-test was used. The Spearman rank correlation coefficient was utilized to investigate whether there were any

significant correlations between individual features across the four parameter maps, thus potentially enabling reduction in the number of features employed in multiparametric modeling. Univariate and correlation analysis were performed using SPSS (IBM SPSS Statistics for Windows, v. 25.0. Armonk, NY) with $P < 0.05$ regarded as significant.

A support vector machine (SVM) binary linear classifier, which facilitates the mapping of inputs into high-dimensional feature spaces, was then utilized to generate classification models, independently based on initial enhancement, overall enhancement, and area under the enhancement curve-derived data. SVMs have previously been employed in MR-based breast classification tasks.[18,26–28] To reduce the possibility of overfitting, only the four most discriminatory texture features were inputted in each model, alongside patient age. All software development and subsequent classification tasks were performed in MatLab (2017b, MathWorks, Natick, MA).

Finally, the efficacy of the developed models was assessed using the previously unseen test dataset and sensitivity, specificity, positive predictive value, and negative predicted values determined.

Results

Parameter maps were successfully calculated for all lesions, examples of which are shown in Fig. 2, illustrating the presence of heterogeneous internal enhancement. With regard to counting statistics for texture analysis the median lesion size was 267 pixels (range 47–1404 pixels).

Univariate analysis on the training dataset revealed a large number of significant differences between benign and malignant lesions for the first-order and textural features calculated from initial enhancement, overall enhancement, and area under the enhancement curve maps. For first-order statistics-based features, 12/15 were significant ($P < 0.050$), 14/48 features were significant for co-occurrence matrices-based features ($P < 0.047$), 25/33 features were significant for run length matrices-based features ($P < 0.050$), and 7/33 features were significant for size zone matrices-based features ($P < 0.043$). Results for first-order statistics and run length matrices-based texture features are illustrated in Tables 3 and 4 by way of example. No significant differences were noted between benign and malignant lesions washout parameter maps-based texture features based on first-order statistics ($P > 0.224$), co-occurrence matrices ($P > 0.221$), run length matrices ($P > 0.418$), size zone matrices ($P > 0.204$), or neighborhood gray tone difference matrices ($P > 0.615$).

No significant differences were found utilizing neighborhood gray tone difference matrices-based features calculated from either initial enhancement, overall enhancement, washout, or area under the enhancement curve parameter maps ($P > 0.131$).

Spearman rank correlation analysis revealed highly significant positive correlations for all texture features across the parameter maps initial enhancement, overall enhancement, and area under the enhancement curve (Table 5 and Fig. 3), indicating that minimal additional discriminatory power is being provided by including features from all three maps in subsequent multivariate analysis.

SVM analysis revealed similar results for the training dataset, whether employing data extracted from initial enhancement maps, overall enhancement maps, or area under the enhancement curve maps in turn (AUCs ranging from 0.75–0.81). AUC values for the test datasets were almost identical to those obtained for the training data, indicating that overfitting is not present (Table 6). For the initial enhancement maps model the features skewness, energy, f_6 (sum average), and low gray run emphasis were used. Skewness, f_6, high gray run emphasis, and long run high gray emphasis were employed in the overall enhancement maps model. Finally, skewness, energy, f_6, and f_8 (sum entropy) were utilized in the model based on area under the enhancement curve maps. All three models also incorporated patient age. High negative (>89%) and positive predictive values (>83%) were found for all three models.

Discussion

This study demonstrated the potential utility of texture analysis in discriminating sub-1 cm benign and malignant breast lesions. Texture parameters calculated from initial enhancement, overall enhancement, and area under the enhancement curve maps appear to offer similar discriminatory power, while texture parameters calculated from washout maps appear to have no diagnostic value for this cohort. The strong correlations noted between texture features calculated across the initial enhancement, overall enhancement, and area under the enhancement curve maps suggest that contrast uptake heterogeneity within lesions does not vary significantly for small breast lesions.

Small breast lesions are usually nonpalpable and the majority are detected via screening, either mammography or MRI. Accurate characterization of such lesions is important both in terms of increasing detection rates and obviating the need for unnecessary biopsies. This work has employed radiomics features determined from contrast-enhanced MR data to address this issue, with the primary goal of classifying these diagnostically challenging lesions. Contrast-enhanced MR can be regarded as a functional imaging technique predicated on blood flow changes in lesions with respect to healthy tissue. As such, it can highlight tumors without solely relying on anatomical changes, resulting in the ability to detect cancers only a few millimeters in size.[29]

A major strength of this work was the complete separation of the training and test datasets, ensuring that the potential for overfitting is minimized. Previous work either involved no further validation of the model developed,[17] or the utilization of all cases in feature selection[18]; both approaches can be considered suboptimal.

The complete lack of discrimination for any of the features determined from washout maps is also worth noting. This indicates that while washout may be present in individual pixels, there is little evidence that the spatial variations in washout pattern are sufficiently distinct between benign and malignant lesions. Previously, it was noted that washout characteristics, calculated using a two-compartment model, do not appear to be particularly useful in the diagnosis of small breast lesions,[17] a finding further confirmed in this work. The lack of discriminatory ability for texture features calculated from washout maps may be reflective of the relatively uniform blood supply across these small lesions, resulting in an absence

of necrosis. With the advent of abbreviated breast MRI protocols, sampling of the latter portion of the enhancement curve, which clearly encompasses washout, is also becoming less prevalent in MRI-based breast screening specifically and breast MRI generally.[30]

An important finding in this study is the observation of highly significant positive correlations between texture features calculated from the initial enhancement, overall enhancement, and area under the enhancement curve maps. This implies that enhancement rates are not varying spatially within the lesion during the sampled time course and that there is little additional value in extending data acquisition beyond the peak of enhancement for this patient cohort. Interestingly, Nagarajan et al[18] also demonstrated no significant improvement in lesion discrimination when considering data from all five postcontrast phases compared with the best two or three postcontrast images.

Traditionally dynamic imaging in the breast has always involved a compromise between the competing requirements of high temporal resolution to appropriately sample the rapid contrast uptake observed and high spatial resolution for detailed lesion morphology. As under sampling techniques, such as compressed sensing, become more widely available, and indeed applied to breast imaging,[31,32] the improved spatial and temporal resolution afforded by these methods have the potential to provide advances in diagnosis, including for small lesions. Higher spatial resolution while maintaining sufficient temporal resolution for pharmacokinetic modeling should enable greater perception of lesion morphology and enhancement characteristics both visually and quantitatively via texture and pharmacokinetic analysis.

It is important to acknowledge that this study has limitations. By only utilizing data from a single center, it is difficult to evince from the presented results how the developed models might perform with data acquired under differing protocols. Particularly, care must be taken when employing data with poorer spatial resolution and slice thickness. Clearly, small lesions do not constitute many pixels in an image with 1.1 mm isotropic spatial resolution, so analyzing data with a decreased spatial resolution may be unviable due to the dominance of partial volume effects. A decreased spatial resolution suggests that there will be fewer pixels in the final ROI, reducing counting statistics and also increasing the proportion of pixels that can be regarded as potentially contaminated by partial volume effects. In this instance the median lesion size was ~270 pixels, so the pragmatic decision was made to decrease the data to only 16 gray levels, as opposed to 32 or 64 gray levels that have previously been employed in breast MR,[33] to ensure adequate counting statistics. However, it is recognized that this reduction to 16 gray levels could potentially obscure important differences between benign and malignant lesions, since discriminatory power must eventually become compromised as the number of gray levels utilized is reduced.

A cohort of 165 lesions is clearly reasonable in size, but splitting the data into distinct training and test sets resulted in a relatively small number of cases for prediction model testing. However, this was deemed necessary, as a split with 66–80% of cases in the training set and 34–20% of cases in the test set is generally advocated. With such a relatively small test dataset it was regarded as prudent to limit the number of features employed in the

prediction models. Thus, the presented prediction models are not necessarily the optimal models for these data, but this is a justifiable approach to reduce potential overfitting.

A final limitation noted is that no attempt to spatially register images acquired at the four timepoints was undertaken, conceivably making the data vulnerable to issues because of patient motion. However, visual inspection of the ROIs across all contrast enhancement phases enabled cases with gross motion artifacts to be eliminated. Undoubtedly, the presence of minor motion artifacts, alongside the small nature of the lesions involved, suggests that the calculated enhancement maps are susceptible to partial volume effects and signal contamination from surrounding parenchymal tissue. However, there is evidence in the literature that peritumoral enhancement is potentially important in breast cancer,[34] so inclusion of such tissue will not necessarily negatively impact the results.

In conclusion, this work demonstrated that radiomics analysis of small contrast-enhancing breast lesions, which are otherwise difficult to categorize, is both feasible and of value. The highly significant strong correlations seen for all texture-based features across the initial enhancement, overall enhancement, and area under the enhancement curve maps suggests that little additional texture information is obtained in imaging for the entire duration of the contrast enhancement curve in this cohort.

Acknowledgment

Contract grant sponsor: NIH/NCI Cancer Center Support; Contract grant number: P30 CA008748; Contract grant sponsor: Susan G. Komen Foundation; Contract grant sponsor: Breast Cancer Research Foundation.

References

1. Fisher B, Slack NH, Bross IDJ. Cancer of the breast: Size of neoplasm and prognosis. Cancer 1969;24:1071–1080. [PubMed: 5353940]
2. Koscielny S, Tubiana M, Lê MG, et al. Breast cancer: Relationship between the size of the primary tumour and the probability of metastatic dissemination. Br J Cancer 1984;49:709–715. [PubMed: 6733019]
3. Laura S, Coombs N, Ung O, Boyages J. Tumour size as a predictor of axillary node metastases in patients with breast cancer. ANZ J Surg 2006;76:1002–1006 [PubMed: 17054550]
4. Sopik V, Narod SA. The relationship between tumor size, nodal status and distant metastases: On the origins of breast cancer. Breast Cancer Res Treat 2018;170:647–656. [PubMed: 29693227]
5. Peters NHGM, Rinkes IHMB, Zuithoff NPA, et al. Meta-analysis of MR imaging in the diagnosis of breast lesions. Radiology 2008;246: 116–124. [PubMed: 18024435]
6. Zhang L, Tang M, Min ZQ, Lu J, Lei XY, Zhang XL. Accuracy of combined dynamic contrast–enhanced magnetic resonance imaging and diffusion–weighted imaging for breast cancer detection: A meta–analysis. Acta Radiol 2016;57:651–660. [PubMed: 26275624]
7. Schlossbauer T, Leinsinger G, Wismuller A, et al. Classification of small contrast enhancing breast lesions in dynamic magnetic resonance imaging using a combination of morphological criteria and dynamic analysis based on unsupervised vector–quantization. Invest Radiol 2007; 43:56–64.
8. Meissnitzer M, Dershaw DD, Feigin K, Bernard-Davila B, Barra F, Morris EA. MRI appearance of invasive subcentimetre breast carcinoma: Benign characteristics are common. Br J Radiol 2017;90: 20170102. [PubMed: 28452624]
9. Kuhl C, Weigel S, Schrading S, et al. Prospective multicenter cohort study to refine management recommendations for women at elevated familial risk of breast cancer: The EVA trial. J Clin Oncol 2010;28: 1450–1457. [PubMed: 20177029]

10. Morris EA, Comstock CE, Lee CH. ACR BI–RADS® Magnetic Resonance Imaging. ACR BI–RADS® Atlas, Breast Imaging Reporting and Data System. Reston, VA: American College of Radiology; 2013.
11. Liberman L, Mason G, Morris EA, Dershaw DD. Does size matter? Positive predictive value of MRI-detected breast lesions as a function of lesion size. AJR Am J Roentgenol 2006;186:426–430. [PubMed: 16423948]
12. Gibbs P, Turnbull LW. Textural analysis of contrast-enhanced MR images of the breast. Magn Reson Med 2003;50:92–98 [PubMed: 12815683]
13. Nie K, Chen J-H, Hon JY, Chu Y, Nalcioglu O, Su M-Y. Quantitative analysis of lesion morphology and texture features for diagnostic prediction in breast MRI. Acad Radiol 2008;15:1513–1525. [PubMed: 19000868]
14. Kim J-H, Ko ES, Lim Y, et al. Breast cancer heterogeneity: MR imaging texture analysis and survival outcomes. Radiology 2016;282:665–675. [PubMed: 27700229]
15. Pickles MD, Lowry M, Gibbs P. Pretreatment prognostic value of dynamic contrast–enhanced magnetic resonance imaging vascular, texture, shape, and size parameters compared with traditional survival indicators obtained from locally advanced breast cancer patients. Invest Radiol 2016;51:177–185. [PubMed: 26561049]
16. Park H, Lim Y, Ko ES, et al. Radiomics signature on magnetic resonance imaging: Association with disease-free survival in patients with invasive breast cancer. Clin Cancer Res 2018;3783.2017.
17. Gibbs P, Liney GP, Lowry M, Kneeshaw PJ, Turnbull LW. Differentiation of benign and malignant sub-1 cm breast lesions using dynamic contrast enhanced MRI. Breast 2004;13:115–121. [PubMed: 15019691]
18. Nagarajan MB, Huber MB, Schlossbauer T, Leinsinger G, Krol A, Wismüller A. Classification of small lesions in breast MRI: Evaluating the role of dynamically extracted texture features through feature selection. J Med Biol Eng 2013;33:59–68.
19. Nagarajan MB, Huber MB, Schlossbauer T, Leinsinger G, Krol A, Wismuller A. Classification of small lesions on dynamic breast MRI: Integrating dimension reduction and out-of-sample extension into CADx methodology. Artif Intell Med 2014;60:65–77. [PubMed: 24355697]
20. Onishi N, Sadinski M, Gallagher KM, et al. Ultrafast dynamic contrast enhanced MRI of the breast using DISCO: Are the quantitative parameters helpful in differentiating between BI-RADS 4 and 5 subcentimeter invasive carcinomas and benign lesions. In: Proceedings of the Joint Annual Meeting ISMRM-ESMRMB, Paris; 2018 (abstract 99).
21. Haralick RM, Shanmugam K, Dinstein I. Textural features for image classification. IEEE Trans Syst Man Cybern 1973;SMC3:610–621.
22. Conners RW, Trivedi MM, Harlow CA. Segmentation of a high-resolution urban scene using texture operators. Comput Vis Graph Image Process 1984;25:273–310.
23. Galloway MM. Texture analysis using gray level run lengths. Comput Vision Graph 1975;4:172–179.
24. Thibault G, Fertil B, Navarro C, et al. Shape and texture indexes application to cell nuclei classification. Int J Pattern Recognit Artif Intell 2013;27:1357002.
25. Amadasun M, King R. Textural features corresponding to textural properties. IEEE Trans Syst Man Cybern 1989;19:1264–1274.
26. Levman J, Leung T, Causer P, Plewes D, Martel AL. Classification of dynamic contrast-enhanced magnetic resonance breast lesions by support vector machines. IEEE Trans Med Imaging 2008;27:688–696. [PubMed: 18450541]
27. Agner SC, Rosen MA, Englander S, et al. Computerized image analysis for identifying triple-negative breast cancer and differentiating them from other molecular subtypes of breast cancer on dynamic contrast-enhanced MR images: A feasibility study. Radiology 2014; 272:91–99. [PubMed: 24620909]
28. Sutton EJ, Dashevsky BZ, Oh JH, et al. Breast cancer molecular subtype classifier that incorporates MRI features. J Magn Reson Imaging 2016;44:122–129. [PubMed: 26756416]
29. Ha R, Sung J, Lee C, Comstock C, Wynn R, Morris E. Characteristics and outcome of enhancing foci followed on breast MRI with management implications. Clin Radiol 2014;69:715–720. [PubMed: 24680120]

30. Mann RM, van Zelst JCM, Vreemann S, Mus RDM, Is ultrafast or abbreviated breast MRI ready for primetime? Curr Breast Cancer Rep 2019;11:9–16.

31. Chan RW, Ramsay EA, Cheung EY, Plewes DB. The influence of radial undersampling schemes on compressed sensing reconstruction in breast MRI. Magn Reson Med 2012;67:363–377. [PubMed: 21656558]

32. Jimenez JE, Strigel RM, Johnson KM, Bancroft LCH; Reeder SB, Block WF. Feasibility of high spatiotemporal resolution for an abbreviated 3D radial breast MRI protocol. Magn Reson Med 2018;80: 1452–1466 [PubMed: 29446125]

33. Ahmed A, Gibbs P, Pickles M, Turnbull L. Texture analysis in assessment and prediction of chemotherapy response in breast cancer J Magn Reson Imaging 2013;38:89–101. [PubMed: 23238914]

34. Braman NM, Etesami M, Prasanna P, et al. Intratumoral and peritumoral radiomics for the pretreatment prediction of pathological complete response to neoadjuvant chemotherapy based on breast DCE-MRI. Breast Cancer Res 2017;19:57. [PubMed: 28521821]

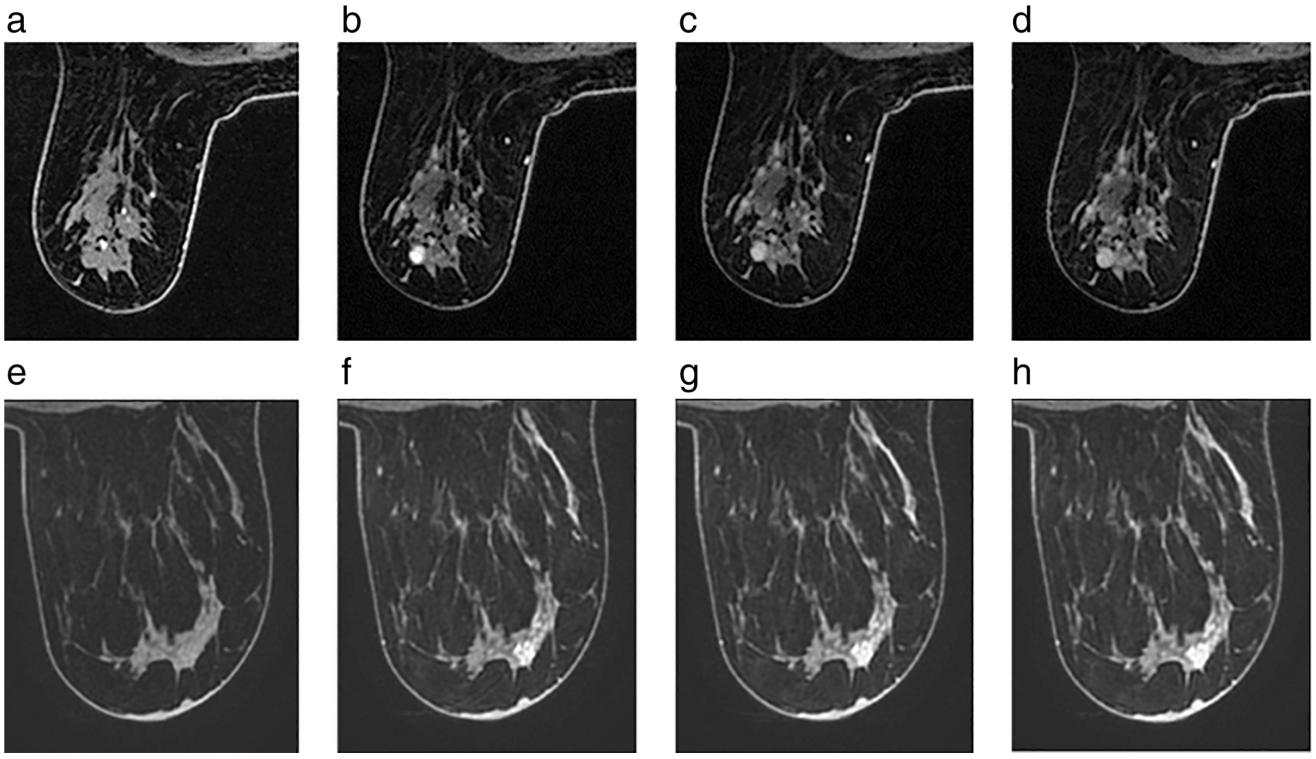

FIGURE 1:
Precontrast **(a,e)** through to final postcontrast image **(d,h)** of a BI-RADS 4 lesion in a 69-year-old woman diagnosed with ipsilateral breast cancer which biopsy subsequently confirmed as a papilloma **(a–d)** and of a BI-RADS 4 lesion in a 39-year-old woman diagnosed with ipsilateral breast cancer which was later confirmed as an invasive ductal carcinoma **(e–h).**

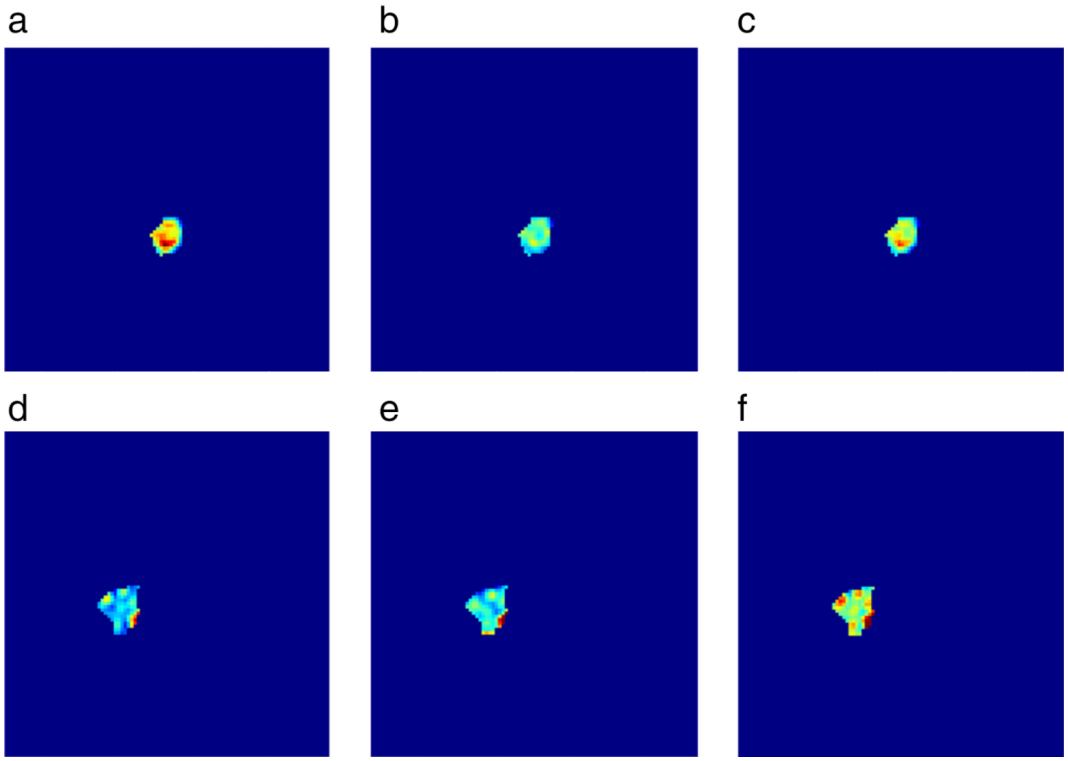

FIGURE 2:

Parameter maps from the two lesions illustrated in Fig. 1. Initial enhancement **(a,d),** overall enhancement **(b,e),** and area under the enhancement curve **(c,f)** maps for a benign papilloma (a–c) and a malignant invasive ductal carcinoma (d–f). It is evident that spatially heterogeneous enhancement is present, which can thus be quantified using texture analysis.

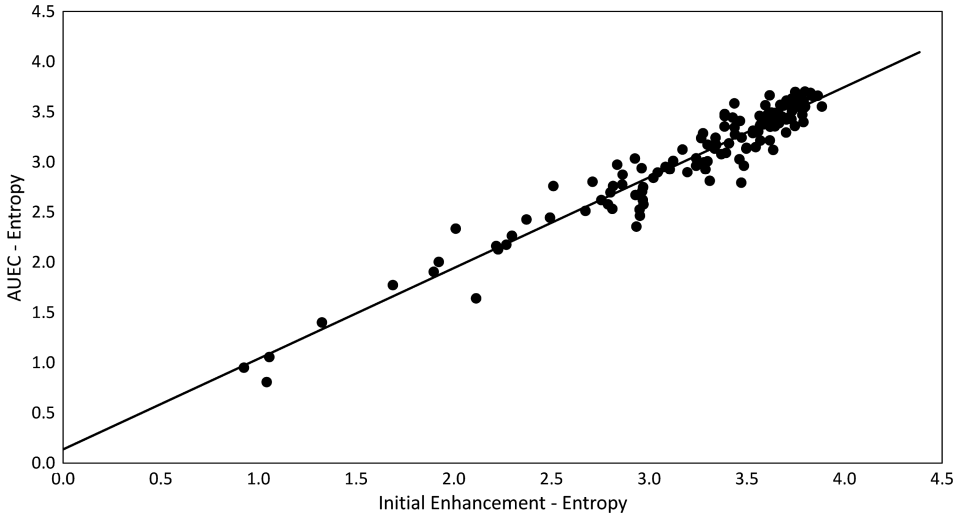

FIGURE 3:

Scatterplot of entropy calculated from area under the enhancement curve maps against entropy calculated from initial enhancement maps, for all lesions utilized in the training dataset. The very high correlation present ($R^2 = 0.927$, $P < 0.001$) suggests that there is limited value in employing information garnered from later points on the contrast enhancement curve compared with the initial high-resolution postcontrast enhancement scan (~100 sec postcontrast injection).

TABLE 1.

Lesion Characteristics

	Total incidence	Training cohort	Test cohort
Malignant lesions	(*n* = 35)	(*n* = 26)	(*n* = 9)
Histopathology			
Invasive ductal carcinoma (IDC)	9 (26%)	7 (27%)	2 (22%)
Invasive lobular carcinoma (ILC)	13 (37%)	9 (35%)	4 (44%)
Mixed IDC & ILC	3 (9%)	3 (12%)	0
Microinvasive carcinoma	1 (3%)	1 (4%)	0
DCIS	9 (26%)	6 (23%)	3 (33%)
Molecular subtype (where available)			
Luminal A/B	23 (66%)	18 (69%)	5 (56%)
Luminal-HER2	1 (3%)	1 (4%)	0
HER2	0	0	0
Triple negative	2 (6%)	1 (4%)	1 (11%)
LN metastasis (where available)			
Positive	3 (9%)	2 (8%)	1 (17%)
Negative	22 (63%)	17 (65%)	5 (83%)
Benign Lesions	(*n* = 130)	(*n* = 98)	(*n* = 32)
Histopathology			
High risk benign lesion	16 (12%)	11 (11%)	5 (16%)
Fibroadenoma	13 (10%)	9 (9%)	4 (13%)
Papilloma	8 (6%)	4 (4%)	4 (13%)
Others	93 (72%)	74 (76%)	19 (59%)

TABLE 2.

Dynamic Contrast-Enhanced Imaging Protocol

	T1w 3D	CE T1w 3D	CE T1w 3D
Orientation	Axial	Axial	Axial
Repetition time (msec)	7.9	3.8	7.9
Echo time (msec)	4.3	1.7	4.3
Flip angle (deg)	12	10	12
Slice thickness (mm)	1.0	1.6	1.0
In-plane resolution (mm×mm)	1.0×1.0	1.6×1.6	1.0×1.0
Matrix size	512×512	256×256	512×512
Number of phases	1	12–15	3
Acquisition time (min:s)	1:30	1:00	4:30

CE, contrast enhanced.

TABLE 3.

Differentiation Between Benign and Malignant Lesions Utilizing First Order-Based Statistics (Significant Differences in Bold)

	Benign lesions	Malignant lesions	*P*-value
IE variance	11.15 (4.17 to 18.55)	5.90 (2.34 to 14.52)	0.137
IE skewness	0.207 (−0.595 to 2.173)	1.132 (−0.112 to 9.592)	**0.022**
IE kurtosis	−0.34 (−1.14 to 8.55)	3.20 (−0.89 to 90.01)	**0.032**
IE energy	0.090 (0.067 to 0.185)	0.146 (0.078 to 0.979)	**0.029**
IE entropy	3.66 (2.77 to 3.95)	3.09 (0.08 to 3.80)	**0.049**
OE variance	9.36 (4.62 to 16.20)	5.64 (2.34 to 11.36)	0.060
OE skewness	0.169 (−0.754 to 2.684)	1.249 (0.365 to 9.592)	**0.004**
OE kurtosis	0.07 (−1.04 to 10.24)	2.734 (−0.13 to 90.01)	**0.010**
OE energy	0.097 (0.075 to 0.222)	0.149 (0.087 to 0.979)	**0.010**
OE entropy	3.56 (2.63 to 3.86)	3.08 (0.08 to 3.70)	**0.008**
AUEC variance	8.01 (4.64 to 11.63)	4.84 (2.14 to 8.29)	0.094
AUEC skewness	0.188 (−.661 to 1.991)	1.487 (0.053 to 9.592)	**0.005**
AUEC kurtosis	−0.43 (−0.99 to 6.81)	2.866 (−0.68 to 90.01)	**0.006**
AUEC energy	0.107 (0.087 to 0.181)	0.159 (0.100 to 0.979)	**0.008**
AUEC entropy	3.45 (2.84 to 3.66)	3.02 (0.08 to 3.46)	**0.009**

Data are median (range). IE, initial enhancement; OE, overall enhancement; AUEC, area under enhancement curve.

TABLE 4.

Differentiation Between Benign and Malignant Lesions Utilizing Run Length Matrices-Based Statistics (Significant Differences in Bold)

	Initial enhancement	Overall enhancement	Washout	Area under the enhancement curve
SRE	0.093	0.055	0.731	**0.046**
LRE	0.096	**0.049**	0.754	**0.046**
LGRE	**0.017**	**0.018**	0.568	**0.013**
HGRE	**0.037**	**0.006**	0.676	**0.014**
SRLGE	**0.039**	**0.025**	0.602	**0.026**
SRHGE	0.050	**0.008**	0.811	**0.016**
LRLGE	**0.035**	**0.011**	0.488	**0.013**
LRHGE	**0.033**	**0.003**	0.418	**0.010**
GLNU	0.922	0.830	0.694	0.976
RLNU	**0.032**	**0.028**	0.676	**0.022**
RP	0.096	**0.045**	0.759	**0.049**

SRE, short run emphasis; LRE, long run emphasis; LGRE, low gray run emphasis; HGRE, high gray run emphasis; SRLGE, short run low gray emphasis; SRHGE, short run high gray emphasis; LRLGE, long run low gray emphasis; LRHGE, long run high gray emphasis; GLNU, gray level non-uniformity; RLNU, run length nonuniformity; RP, run percentage.

TABLE 5.

Correlation Between Run Length Matrices-Based Texture Features Calculated From Initial Enhancement, Overall Enhancement, and Area Under the Enhancement Curve Parameter Maps

Run length matrix parameter	Initial enhancement *cf.* overall enhancement	Initial enhancement *cf.* area under the enhancement curve	Overall enhancement *cf.* area under the enhancement curve
SRE	0.861	0.938	0.913
LRE	0.873	0.943	0.935
LGRE	0.839	0.925	0.920
HGRE	0.872	0.938	0.911
SRLGE	0.817	0.924	0.899
SRHGE	0.865	0.932	0.901
LRLGE	0.841	0.913	0.939
LRHGE	0.843	0.937	0.897
GLNU	0.978	0.992	0.990
RLNU	0.968	0.989	0.985
RP	0.874	0.946	0.929

All correlations were significant at the 0.01 level. SRE, short run emphasis; LRE, long run emphasis; LGRE, low gray run emphasis; HGRE, high gray run emphasis; SRLGE, short run low gray emphasis; SRHGE, short run high gray emphasis; LRLGE, long run low gray emphasis; LRHGE, long run high gray emphasis; GLNU, gray level non-uniformity; RLNU, run length nonuniformity; RP, run percentage.

TABLE 6.

Performance Characteristics of the Three Independent Prediction Models

	Training set	Test set				
Parameter maps	**AUEC (±SE)**	**AUEC (±SE)**	**Sensitivity**	**Specificity**	**NPV**	**PPV**
IE	0.75 (0.06)	0.78 (0.12)	67%	100%	91%	100%
OE	0.81 (0.05)	0.78 (0.10)	56%	97%	89%	83%
AUEC	0.77 (0.06)	0.76 (0.11)	67%	97%	91%	86%

IE, initial enhancement; OE, overall enhancement; AUEC, area under the enhancement curve; SE, standard error; NPV, negative predictive value; PPV, positive predictive value.

IE map features – age, skewness, energy, f_6 (sum average), low gray run emphasis

OE map features – age, skewness, f_6, high gray run emphasis, long run high gray emphasis

AUEC map features – age, skewness, energy, f_6, f_8 (sum entropy).

J Magn Reson Imaging. Author manuscript; available in PMC 2021 October 08.